Structural and electrical characterisation of ion-implanted strained Silicon

K.Horan[1], A. Lankinen[2], L. O'Reilly[1] N. S. Bennett[3, 4], P.J. McNally[1], B.J. Sealy[4], N.E.B. Cowern[3], T.O. Tuomi[2]

[1]*Nanomaterials Processing Laboratory, Research Institute for Networks and Communications Engineering (RINCE), School of Electronic Engineering, Dublin City University, Dublin 9, Ireland*

[2] *Micro and Nanosciences, Micronova, Helsinki University of Technology, P.O. Box 3500, FIN-02015 TKK, Finland*

[3] *School of Electronic, Electrical and Computer Engineering, University of Newcastle, Newcastle upon Tyne, NE1 7RU, UK*

[4]*Advanced Technology Institute, University of Surrey, Guildford, GU2 7XH, UK*

Abstract

The production of low resistance ultra-shallow junctions for e.g. source/drain extensions using low energy ion-implantation will be required for future CMOS devices [1]. This architecture will require implants which demonstrate high electrical activation and nm range depth profiles. We investigate the properties of Sb implants in tensile strained silicon due to their potential to satisfy these criteria, and the carrier mobility enhancements associated with tensile strained silicon. Low energy (in this case 2 keV) implants coupled with Sb's large atomic radius are capable of providing ~ 10 nm implant depths. In addition to this, Sb, in the presence of tensile strain demonstrates higher electrical activation when compared with the more traditional n-type dopant As [2].

We now report on the initial results of an ongoing systematic study over a wide silicon tensile strain range (from 0.4 to 1.25 % strain) in order to establish clear strain-related trends. Graded $Si_{1-x}Ge_x$ virtual substrates (VS) with $0.1 \le x \le 0.3$ are used as template substrates, upon which tensile strained Si layers are grown. Prior to implantation the

quality of the strained layer and SiGe buffer is assessed using UV micro-Raman spectroscopy (μRS), synchrotron x-ray topography (SXRT) and high resolution x-ray diffraction (HR-XRD). For measurements of strain following implantation, HR-XRD is found to be more useful than μRS due to additional carrier-concentration induced Si Raman peak shifts in the Raman spectra , these obscure small changes in the strain state, and result from the degenerate doping levels achieved in these samples (~$7x10^{20}$ cm^{-3}). Using x-ray techniques, we find clear evidence of tilt in the SiGe VS at Ge concentrations > 23% (i.e. $\varepsilon > 0.9$ %), this tilt impacts on the quality of the strained Si. In addition to this, stacking faults have been detected non-destructively in the higher strain samples ($\varepsilon = 1.25\%$, VS = $Si_{0.7}Ge_{0.3}$) using SXRT in transmission mode.

Acknowledgement

Science Foundation Ireland is gratefully acknowledged for funding this project under the Investigator Programme Grant Scheme Project 05/IN/I656.We acknowledge HASYLAB and the European Community for funding under Contract RII3-CT-2004_506009 (IA-SFS). We are grateful to T. Wroblewski and C. Paulmann for their help at HASYLAB beamline F-1.

1. Introduction

The scaling of the CMOS transistor has been the primary driving factor in the performance improvements, and decreasing power consumption, of integrated circuits [3]. The continuation of these improvements will require the production of ultra-shallow junctions for the source/drain extension regions using low energy ion implantation [1]. Strain engineering using Si/SiGe heterostructures has become a key technology for the enhancement of device operating speeds [4]. Biaxial tensile strain results in the reduction of the sheet resistance (R_s) of highly doped n-type layers created by a low energy (2 keV) As or Sb ion implantation. The effect is more pronounced for Sb, when R_s lowering results not only from strain enhanced mobility, but also from an improvement in Sb solubility with strain present [2]. In a comparison between Sb implants in bulk and strained Si, we found that a 0.7% tensile strain results in a more than doubling of electrically active Sb subject to a low thermal budget rapid thermal anneal (RTA) of 600^oC – 800^oC. The fact that these enhancements are independent of scaling alleviates some of the pressures associated with the impending technological and fundamental limitations of device down-sizing [5]. In order for these two methods of performance enhancement to work in concert, it is necessary to gain an understanding of the effects of strain on dopant diffusion and activation at high dopant concentrations.

2. Experimental Details

Strained silicon epilayers were grown to thicknesses ranging between 9 nm and 42 nm. Wafers were implanted with a 2 keV Sb or As ion dose of between $1x10^{14}$ cm^{-2} and $10x10^{14}$ cm^{-2} creating a junction at a depth of around 10 nm in each case. Control samples were prepared using conventional p-type Si wafers for comparison. The implanted dose was measured by Rutherford back-scattering (RBS). Dopant activation was achieved by RTA of the wafer pieces for 10 seconds in N_2 in the range 600-800^{o}C.

The quality of the SiGe substrates was investigated using white beam synchrotron x-ray topography. The SXRT measurements were performed at the Hamburger Synchrotronstrahlungslabor am Deutschen Elektronen-Synchrotron (HASYLAB-DESY) utilising the continuous spectrum of synchrotron radiation from the DORIS storage ring bending magnet. The ring operates at positron energies of 4.45 GeV and at typical currents of 80-150 mA. Room temperature micro-Raman measurements were performed with a Jobin Yvon LabRam HR800 system in backscattering geometry using a 325 nm He-Cd UV laser excitation with a spot size of approximately 1μm. High-resolution X-ray diffraction (HR-XRD) measurements were performed on a Philips X'Pert Pro diffractometer. Reciprocal space maps (RSM) were collected with a three-bounce germanium analyzer crystal placed before the detector, which narrows the acceptance angle to approximately 12 arc sec. Peak carrier concentrations were measured by the differential Hall profiling technique [2].

3. Results and Discussion

Micro-Raman Spectroscopy

In performing the μRS measurements additional procedural steps were taken. Before measurement, the silicon Raman peak amplitude was normalised to that of the calibration peak by means of accumulation-time scaling. Post measurement, the peak positions were adjusted with reference to the 332 nm neon emission line. These additional experimental steps resulted in a reduction of the measurement error by almost an order of magnitude to ~ 0.1 cm^{-1} [6].

In a related paper [7] we have shown that the usefulness of micro-Raman spectroscopy as a strain metrology tool becomes limited under conditions of high carrier concentration. This is due to the interaction between the discrete Raman transitions and the continuous free-electron excitations at high carrier concentrations [8-10]. The result of this is a direct dependence of the Si Raman peak shifts on carrier concentration and figure 1 gives an example of this.

Figure 1 shows a plot of the Si Raman peak shift for 0.7% tensile strained Si samples annealed at 600^{o}C, 700^{o}C and 800^{o}C, relative to their respective as implanted samples, as a function of carrier concentration. This data shows a clear correlation between these two properties. Due to this dependence, μRS is a less effective tool for strain metrology at high carrier concentrations and therefore complementary techniques such as HR-XRD are required for the task under these conditions. Raman spectroscopy however remains a reliable and quick method of measuring material strain in unimplanted samples.

Figure 2 shows the tensile strain calculated from measurements of the shift in the silicon Raman peak position for samples with Ge substrate content ranging between 10% and 30%. The strain is calculated using the equation,

$$\sigma_{xx} = \sigma_{yy} = \frac{-\triangle\omega_{SiUV}}{4} \text{ (GPa)} \qquad \text{[11-12],} \qquad (1)$$

where σ_{xx} and σ_{yy} are the strains in the x and y directions and $\Delta\omega_{SiUV}$ is the strain induced shift in the Raman peak position. The theoretical strains resulting from the appropriate substrate Ge contents are also plotted, under the assumption of 100 % relaxation in the VS, these are calculated using the equation,

$$\sigma_{Si} = \frac{E_f m}{1-\upsilon} \text{ (GPa)} \qquad \text{[13],} \qquad (2)$$

where E_f and υ are the Young's modulus and Poisson's ratio of the film, respectively, and m is the lattice misfit between the relaxed virtual substrate and the strained silicon layer. Figure 2 reveals a very good agreement between the theory and practice, as all data points but one lie within the experimental error of the theoretical maximum strain. We also observe no appreciable strain relaxation in the super critically thick $Si_{0.7}Ge_{0.3}$ samples (tensile strained silicon layer thicknesses of 12 nm and 15 nm). This suggests that at least initially these structures are meta-stable which allows the inclusion of the complete implant profile within the strained silicon epilayer.

Synchrotron X-Ray Topography and HR-XRD

By way of example figure 3 shows a $1\bar{1}7$ large area back reflection topograph of the strained silicon sample grown on the $Si_{0.77}Ge_{0.23}$ substrate. The entire SiGe buffer layer (~

3 μμ) is imaged here as the x-ray penetration depth (t_p) for this $1\bar{1}7$ reflection is 15.8 μm. Two major features of note are observed in the topograph. Firstly, the crosshatched pattern running along two perpendicular <110> directions is an image of the array of misfit dislocations (MD) common in strained silicon samples [14]. These MDs are the most likely mechanism in providing strain relaxation in the VS, necessary for stable strained silicon epilayer growth. This strain relaxation is further confirmed by reciprocal space map (RSM) data. These misfit dislocations are observed in all samples. The second feature in the topograph is the presence of a lighter intensity overlapping diffraction image, labelled "S" in figure 3. This displaced image indicates that a region of the SiGe buffer is tilted with respect to the substrate, this tilting results in a different Bragg angle for this region and therefore a slight displacement on the recording film. This tilt is further confirmed by HR-XRD. Figure 4 shows the 224 RSM in the $(1\bar{1}0)$ diffraction plane. This RSM shows four peaks in the SiGe buffer caused by the terraced graded growth method employed in fabricating these samples and a fifth, intense SiGe peak, at the maximum Ge concentration of 23%. The fact that the in-plane reciprocal position of the uppermost of these lies to the right of the silicon substrate peak in the RSM is a result of tilt in the SiGe buffer layer. This tilt can be quantified by examining the 004 omega (ω) scans in the (110), $(\bar{1}\bar{1}0)$, $(\bar{1}10)$ and $(\bar{1}10)$ diffraction planes in accordance with the technique laid out by Nagai [15]. It was found that just above the substrate the SiGe graded layer demonstrates a tilt of 0.16^o toward the [110] lattice plane and that this reduces to ~ 0.1^o at the start of the strained silicon epilayer. A tilt of ~ 0.11^o was measured at the uppermost terrace of the SiGe graded layer accounting for its initially

anomalous position. An important caveat is that Nagai's theory no longer holds after the formation of MDs; this may account for the reduction in the tilt as the MDs act to not only reduce strain but also lattice tilt. The strained silicon lateral lattice constant can also be seen to be in good agreement with the SiGe buffer in figure 4 as their x- and y-reciprocal space positions can be seen to be the same. Initial HR-XRD data suggests that greater tilt angles are observed for higher Ge concentrations in the VS, reaching a maximum for $Si_{0.7}Ge_{0.3}$ substrate, this is line with theory as the degree of tilt is dependent on the lattice mismatch [15].

Figure 5 shows a large area transmission topograph of the strained silicon sample grown on a 30% Ge substrate. The large "box-like" structures bounded by misfit dislocations are indicative of stacking faults (SF) [16]. The clarity of these X-ray topographic SF images suggests that the crossing stacking faults are not interfering with each other. We speculate that this may be a result of the graded nature of the SiGe buffer, which can confine MD arrays and SFs to individually grown terraces and this can allow SF to pass under and over each other. The white "boxes" which can be seen in figure 5 may be a result of an even number of SF with symmetrically opposite Burgers vectors passing through the imaged region. In this case the two diffracted x-ray wave-fronts could undergo phase-shifts in opposite directions resulting in no net change. For example, four stacking faults on top of each other, bordered by 60^{o} misfit dislocations having the same Burgers vectors, may produce a contrast similar to that imaged in figure 5.

4. Conclusion

μRS, SXRT and HR-XRD were used to study the stability of highly strained tensile silicon layers doped with Sb, grown on $Si_{1-x}Ge_x$ virtual substrates. For unimplanted samples μRS continues to be of major benefit for strain metrology. The Raman data collected here shows the strain present in these samples to be close to the theoretical maximum strain for these structures. We also see that at least initially, structures grown to thicknesses beyond their theoretical critical thickness are meta-stable. SXRT topographs reveal the presence of misfit dislocations in all samples confirming the presence of a relaxed VS for all Ge concentrations. The emergence of lattice tilts at VS Ge contents above ~ 23% have been detected in both SXRT and HR-XRD measurements, and this may be of technological concern as this tilt continues into the strained silicon layer. At a VS Ge content of ~30% stacking faults have been imaged using SXRT. These appear to be confined by the misfit dislocations in the SiGe VS. However, if these were to reach the strained silicon layer they could cause major problems for any device structure built on this material and future studies will focus on the thermal stability of these.

References

(1) Wakabayashi, H., Ueki, M., Narihiro, M., Fukai, T., Ikezawa, N., Matsuda, T., Yoshida, K., Takeuchi, K., Ochiai, Y., Mogami, T., Kunio, T. *Transactions On Electron Devices* **2002***, 49*, 89-94.

(2) Bennett, N. S.; Cowern, N. E. B., Smith, A. J., Gwilliam, R. M., Sealy, B. J., O'Reilly, L., McNally, P. J., Cooke, G., Kheyrandish, H. *Appl. Phys. Lett.* **2006***, 89*, 182122.

(3) Ieong, M., Doris, B., Kedzierski, J., Rim, K., Yang, M. *Science* **2004***, 306*, 2057-2060.

(4) Lee, M. L., Fitzgerald, E. A., Bulsara, M. T., Currie, M. T., Lochtefeld, A. *J. Appl. Phys.* **2005***, 97*, 011101.

(5) Iwai, H. *Solid-State Circuits, IEEE Journal of Solid-State Circuits* **1999***, 34*, 357-366.

(6) Horan, K., O'Reilly, L., Bennett, N. S., McNally, P. J., Sealy, B. J., Cowern, N. E. B. *Optimization of UV-Raman Spectroscopy Analysis of Ultra-Shallow Junctions in Strained Silicon;* IOM3 3rd International Conference on Nanomaterials and Nanomanufacturing 2007; .

(7) O'Reilly, L., Horan, K., McNally, P. J., Bennett, N. S., Cowern, N. E. B., Lankinen, A., Sealy, B. J., Gwillian, R. W., "Constraints on micro-Raman strain metrology for highly doped strained silicon materials", Applied Physics Letters, (in the press).

(8) Cerdeira, F., Cardona, M. *Phys. Rev. B* **1972***, 5*, 1440.

(9) Chandrasekhar, M., Cardona, M., Kane, E. O. *Phys. Rev. B* **1977***, 16*, 3579.

(10) Chandrasekhar, M., Renucci, J. B., Cardona, M. *Phys. Rev. B* **1978***, 17*, 1623.

(11) O'Reilly, L., Bennett, N. S., McNally, P. J., Sealy, B. J., Cowern, N. E. B.; *Micro-Raman study of anomalous dopant-induced behavior in ultra-shallow As and Sb doped strained Si;* International Workshop on INSIGHT in Semiconductor Device Fabrication, Metrology, and Modeling (INSIGHT-2007); 2007; .

(12) De Wolf, I. *Semiconductor Science and Technology* **1996***, 11*, 139-154.

(13) Perova, T. S., Lyutovich, K., Kasper, E., Waldron, A., Oehme, M., Moore, R. A. *Materials Science and Engineering: B,* **2006***, 135*, 192-194.

(14) Koehler, R., Raidt, H., Neumann, W., Pfeiffer, J. U. *Journal of Physics D: Applied Physics* **2005***, 38*, 319-327.

(15) Nagai, H. *J. Appl. Phys.* **1974***, 45*, 3789-3794.

(16) Authier, A. In *Dynamical Theory of X-Ray Diffraction;* Oxford University Press Inc.: New York, 2001; .

List of Figure Captions

Figure 1.

Post anneal Raman shift as a function of carrier concentration. Results are shown for strained silicon samples with 0.7% strain implanted with Sb with doses in the range between $1x10^{14}$ and $1x10^{15}$ and annealed for 10 seconds at 600°C, 700°C and 800°C.

Figure 2.

Measured strain and theoretical maximum strain as a function of Ge substrate content. Lines represent the measured strain and theoretical maximum strain for below critical thickness silicon epilayers, points represent measurements performed on samples with thicknesses above critical thicknesses.

Figure 3.

Large area back reflection topograph of a $Si_{0.77}Ge_{0.23}$ substrate and a 12 nm strained silicon epilayer. The reflection shown is the $1\bar{1}7$ reflection with a penetration depth of 15.8 μm. The film-to-sample distance was 80 mm. The topograph was recorded at HASYLAB-DESY synchrotron under white-beam conditions. The projection of the diffraction vector **g** onto the plane of the recording film is also indicated.

Figure 4.

224 reciprocal space map (RSM) in the $(1\bar{1}0)$ diffraction plane of the 23% Ge substrate sample with 12 nm strained silicon epilayer. Intensity doubles between contour lines.

Figure 5.

Large area transmission topograph of the $Si_{0.3}Ge_{0.7}$ substrate with a 9 nm strained silicon epilayer. The topograph was recorded at HASYLAB-DESY synchrotron under white-beam conditions with a film-to-sample distance of 80 mm. The projection of the diffraction vector **g** onto the plane of the recording film is also indicated.

Figures

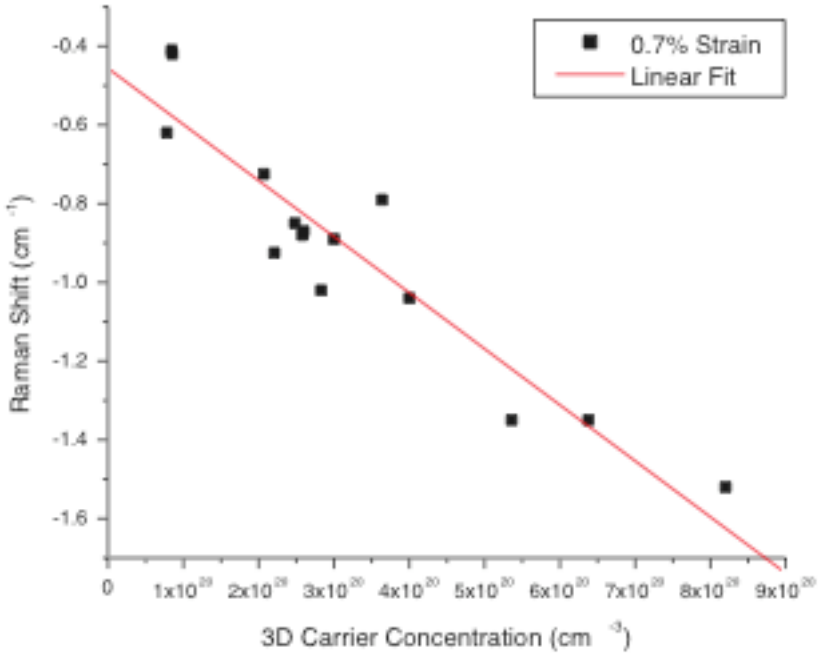

Figure 1.

Post anneal Raman shift as a function of carrier concentration. Results are shown for strained silicon samples with 0.7% strain implanted with Sb with doses in the range between $1x10^{14}$ and $1x10^{15}$ and annealed for 10 seconds at 600°C, 700°C and 800°C.

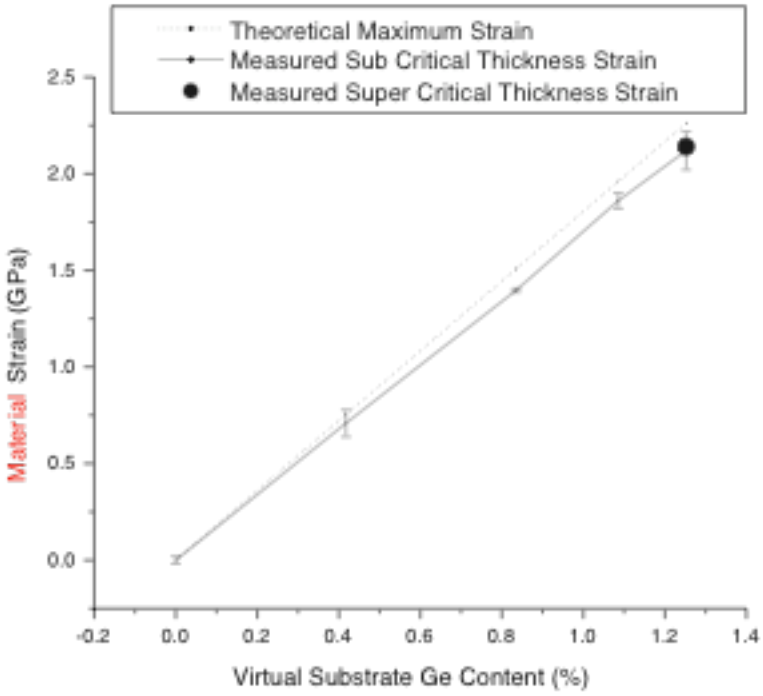

Figure 2.

Measured strain and theoretical maximum strain as a function of Ge substrate content. Lines represent the measured strain and theoretical maximum strain for below critical thickness silicon epilayers, points represent measurements performed on samples with thicknesses above critical thicknesses.

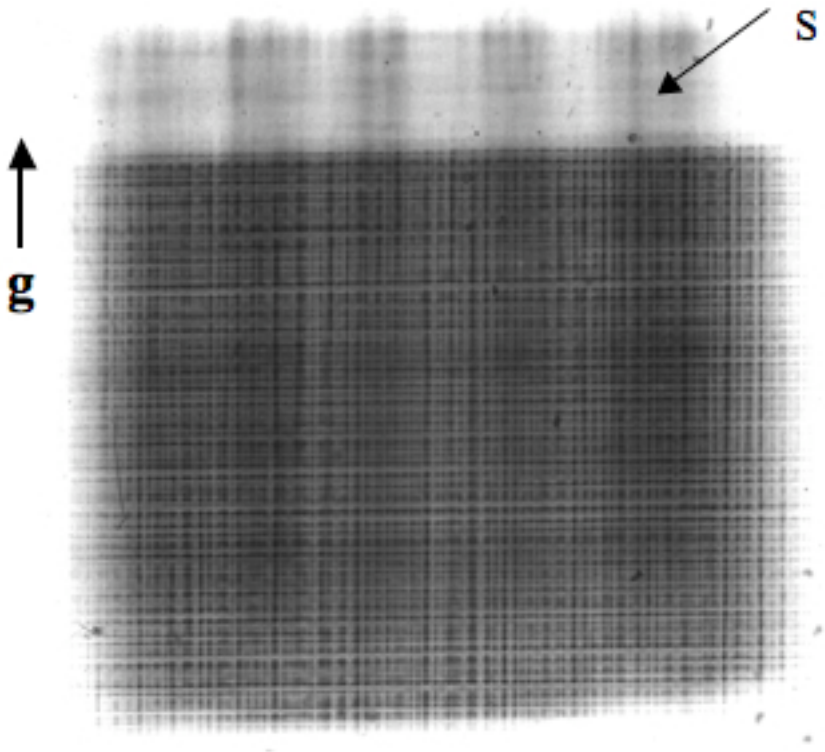

Figure 3.

Large area back reflection topograph of a $Si_{0.77}Ge_{0.23}$ substrate and a 12 nm strained silicon epilayer. The reflection shown is the $1\bar{1}7$ reflection with a penetration depth of 15.8 μm. The film-to-sample distance was 80 mm. The topograph was recorded at HASYLAB-DESY synchrotron under white-beam conditions. The projection of the diffraction vector **g** onto the plane of the recording film is also indicated.

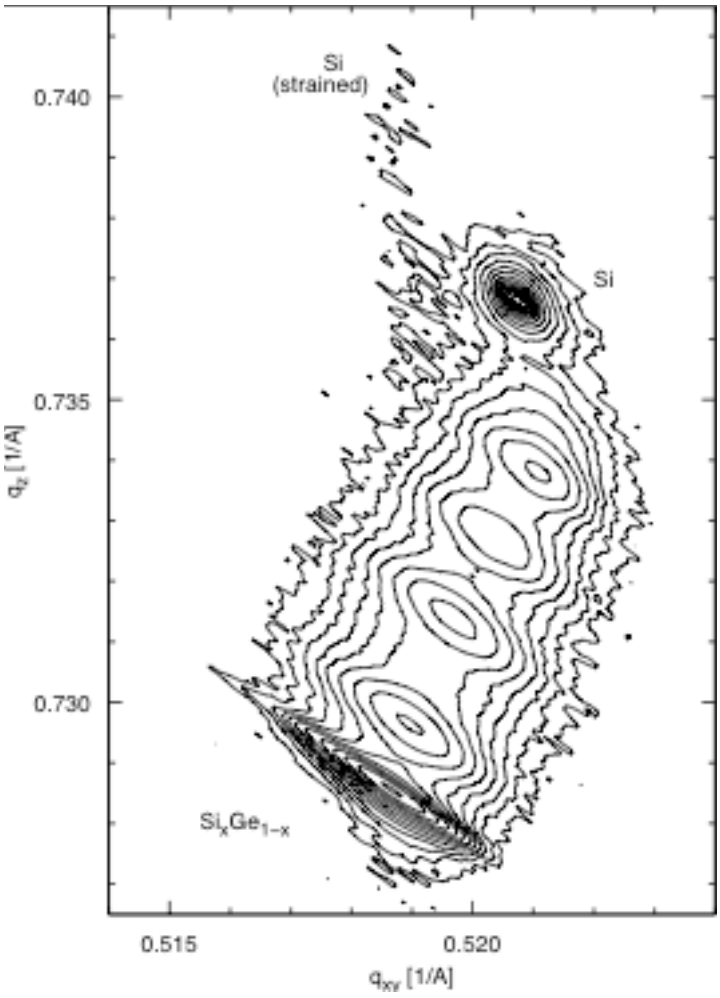

Figure 4.

224 reciprocal space map (RSM) in the $(1\bar{1}0)$ diffraction plane of the 23% Ge substrate sample with 12 nm strained silicon epilayer. Intensity doubles between contour lines.

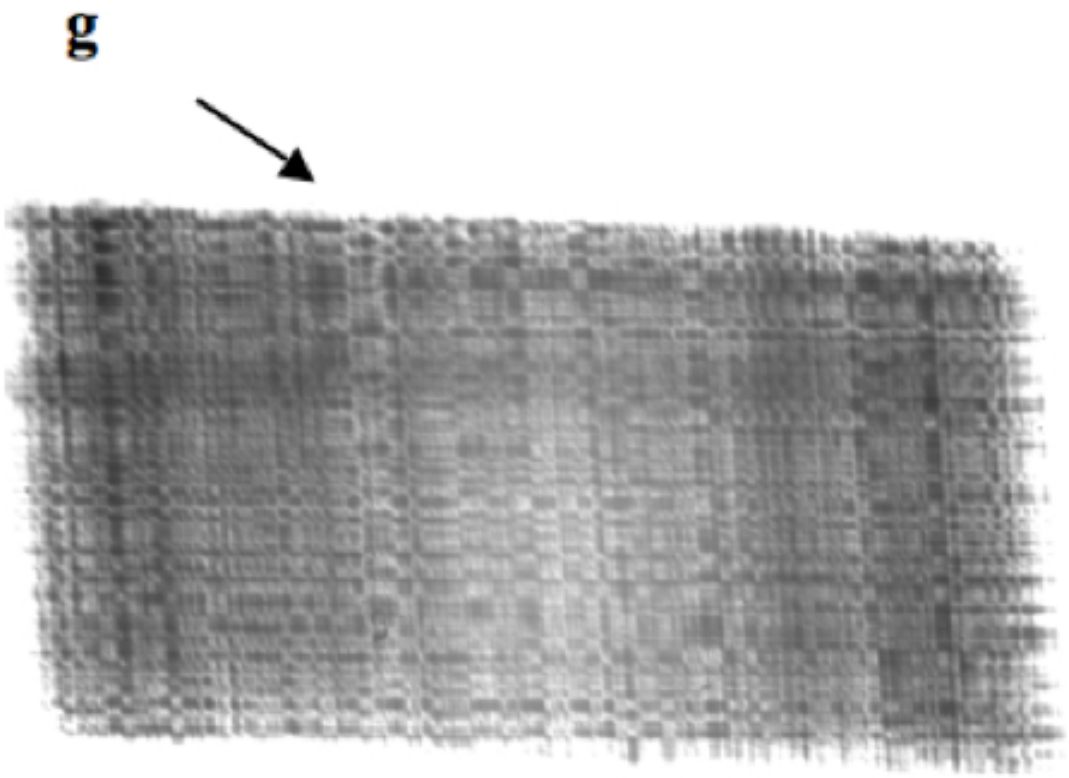

Figure 5.

Large area transmission topograph of the $Si_{0.3}Ge_{0.7}$ substrate with a 9 nm strained silicon epilayer. The topograph was recorded at HASYLAB-DESY synchrotron under white-beam conditions with a film-to-sample distance of 80 mm. The projection of the diffraction vector **g** onto the plane of the recording film is also indicated.